Supplemental material

Alvarez-Baron et al., https://doi.org/10.1085/jgp.201812031

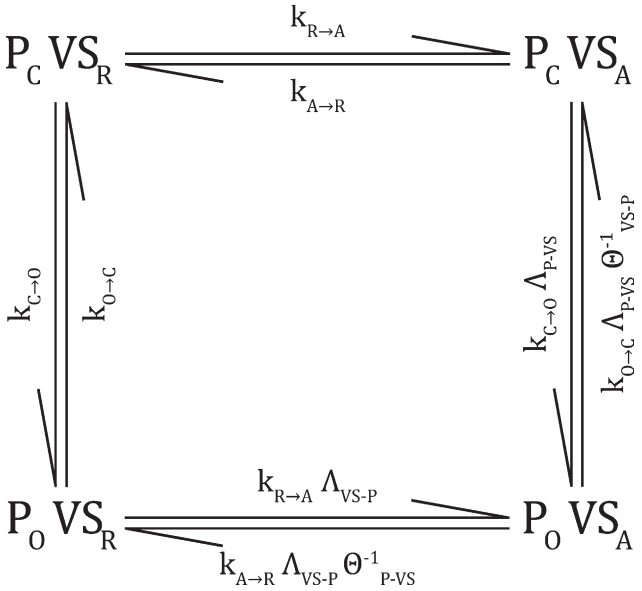

Figure S1. **Kinetic scheme representing interacting binary elements for pore and voltage sensor.** The transition rates to open and close the pore (P) while the voltage sensor (VS) is resting ($k_{C\to O}$ and $k_{O\to C}$, respectively) are modified by interaction factors $\Lambda_{P\text{-}VS}$ and $\Theta_{VS\text{-}P}$ to give the transition rates for the pore when the voltage sensor is activated (denoted $k'_{C\to O}$ and $k'_{O\to C}$ in Materials and methods). The transition rates to activate or deactivate the voltage sensor while the pore is closed ($k_{R\to A}$ and $k_{A\to R}$, respectively) are multiplied by interaction factors $\Lambda_{VS\text{-}P}$ and $\Theta_{P\text{-}VS}$ to obtain the transition rates for the voltage sensor when the pore is open.

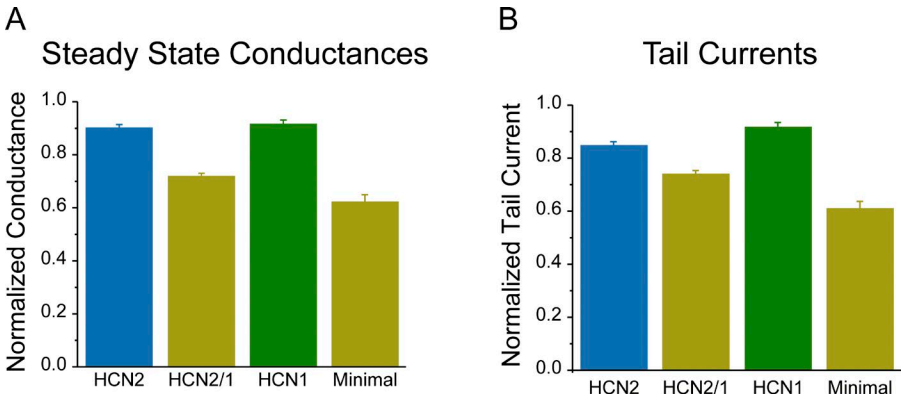

Figure S2. **The maximal conductance at saturating voltages in HCN channels is smaller in the absence than in the presence of cAMP. (A)** Maximal conductance measured at the end of the 3 s activation pulses for WT HCN2, WT HCN1, the HCN2/1 chimera, and the $HCN1_{minimal}$ mutant. Maximal conductances for individual patches were obtained from Boltzmann fits of the conductance–voltage curves and were normalized to the maximal conductance in the presence of cAMP. **(B)** Same as in A, but for the tail currents (data shown in Fig. 4 C). Data presented are mean ± SEM.

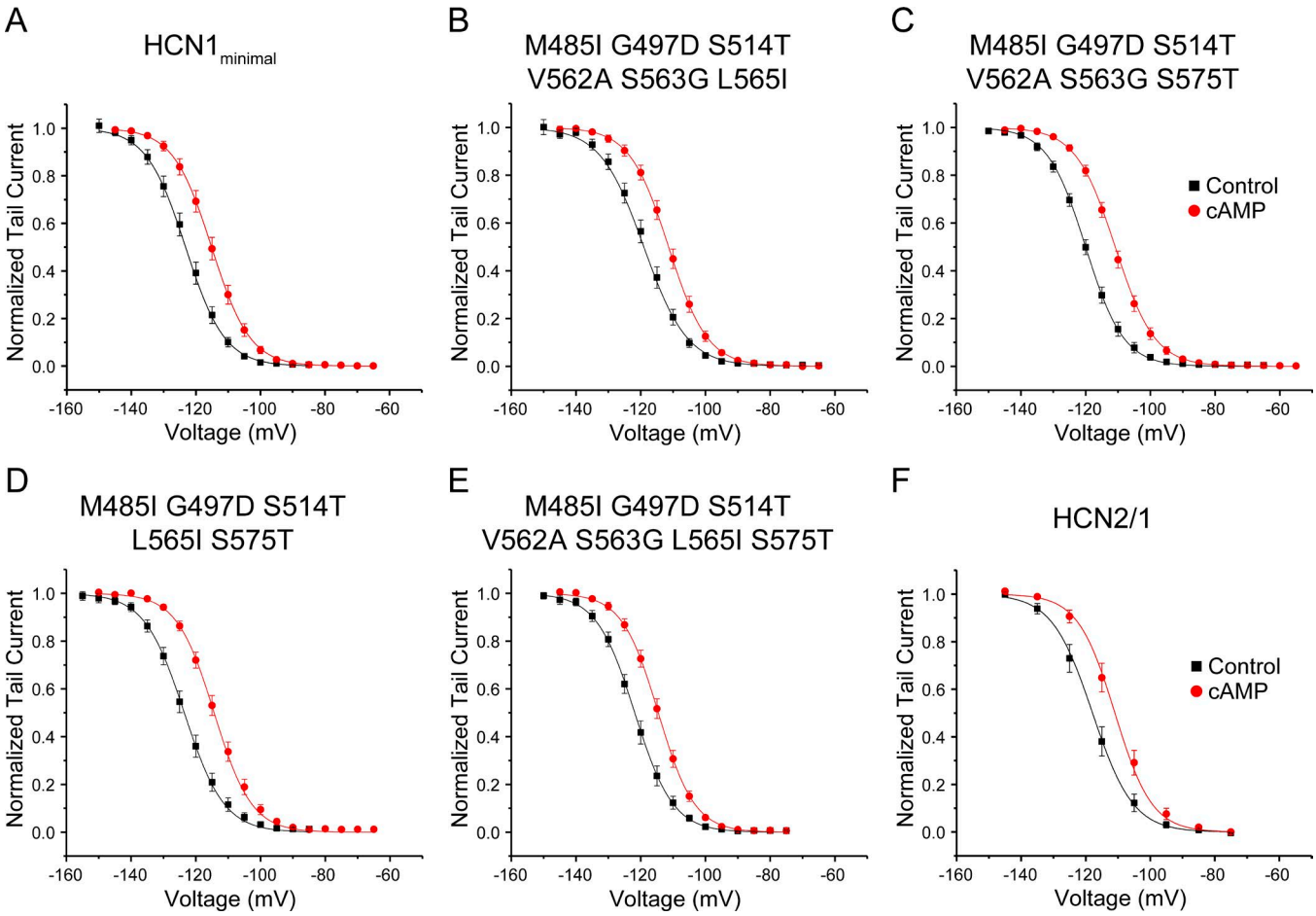

Figure S3. **Additional mutations L565I and S575T do not affect cAMP-dependent $\Delta V_{1/2}$ in the $HCN1_{minimal}$ background. (A–E)** Conductance–voltage curves determined from tail currents for combinations of V562A/S563G, L565I, and S575T. The small shift in activation induced by cAMP in the $HCN1_{minimal}$ mutant (A) was not altered by the addition of L565I (B), S575T (C), or both (E). A combination of L565I and S575T in the absence of V562A/S563G (D) did not produce a reduction in the shift in activation comparable to the $HCN1_{minimal}$ mutant. **(F)** The conductance–voltage curve of the HCN2/1 chimera is shown for comparison. Data presented are mean ± SEM.

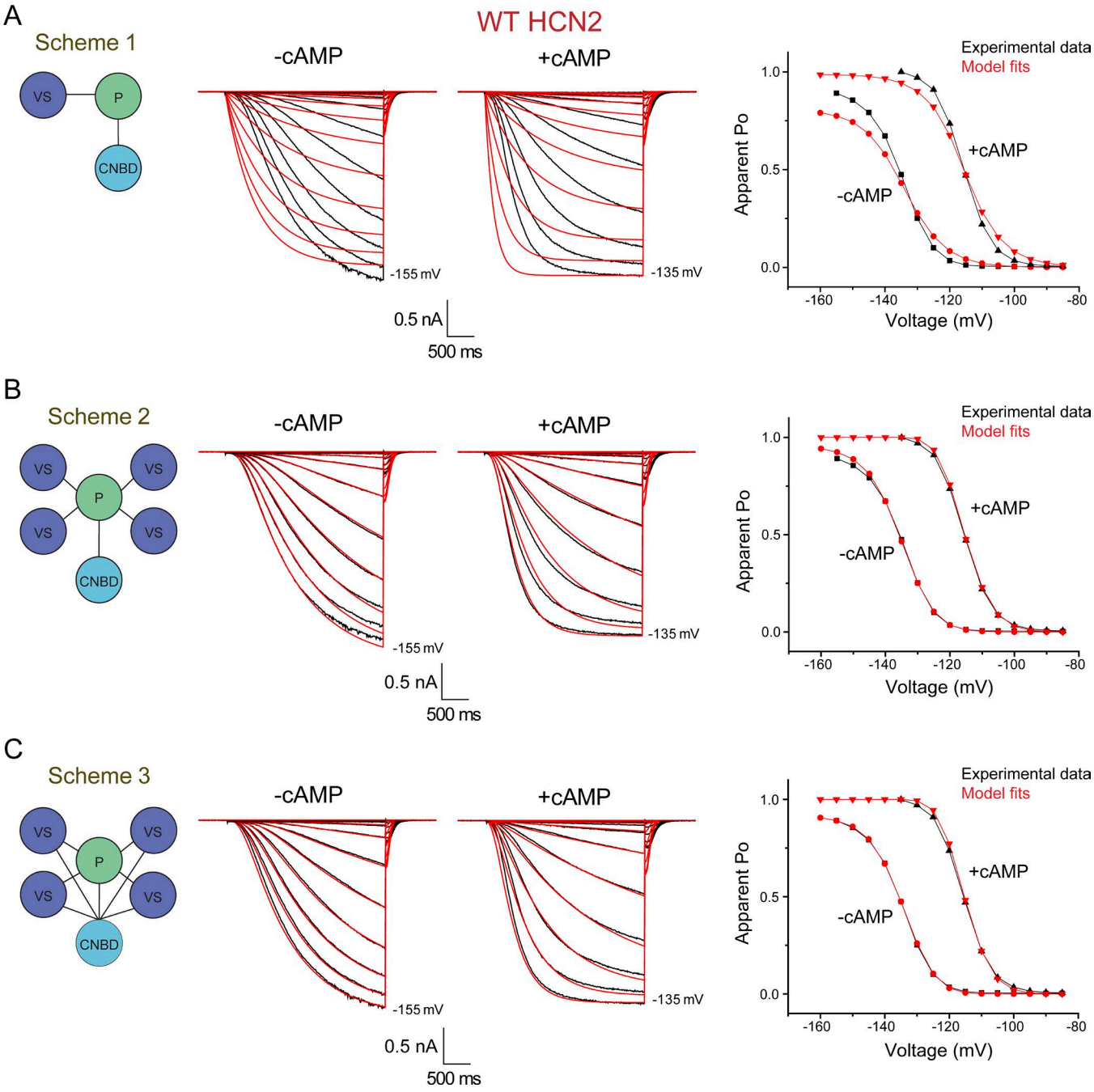

Figure S4. **Allosteric models of voltage- and ligand-dependent gating in WT HCN2 without a linker module.** Schematic representation of the elements and interactions implemented in Schemes 1 (A), 2 (B), and 3 (C). Model fits (red) and experimental data (black) for current traces in response to a voltage pulse protocol illustrating the activation kinetics in the presence and absence of a saturating concentration of cAMP. Reference data for the conductance–voltage curves (right) were obtained from the steady-state conductances calculated at the end of each pulse and are compared with the probability of the open state calculated from the model.

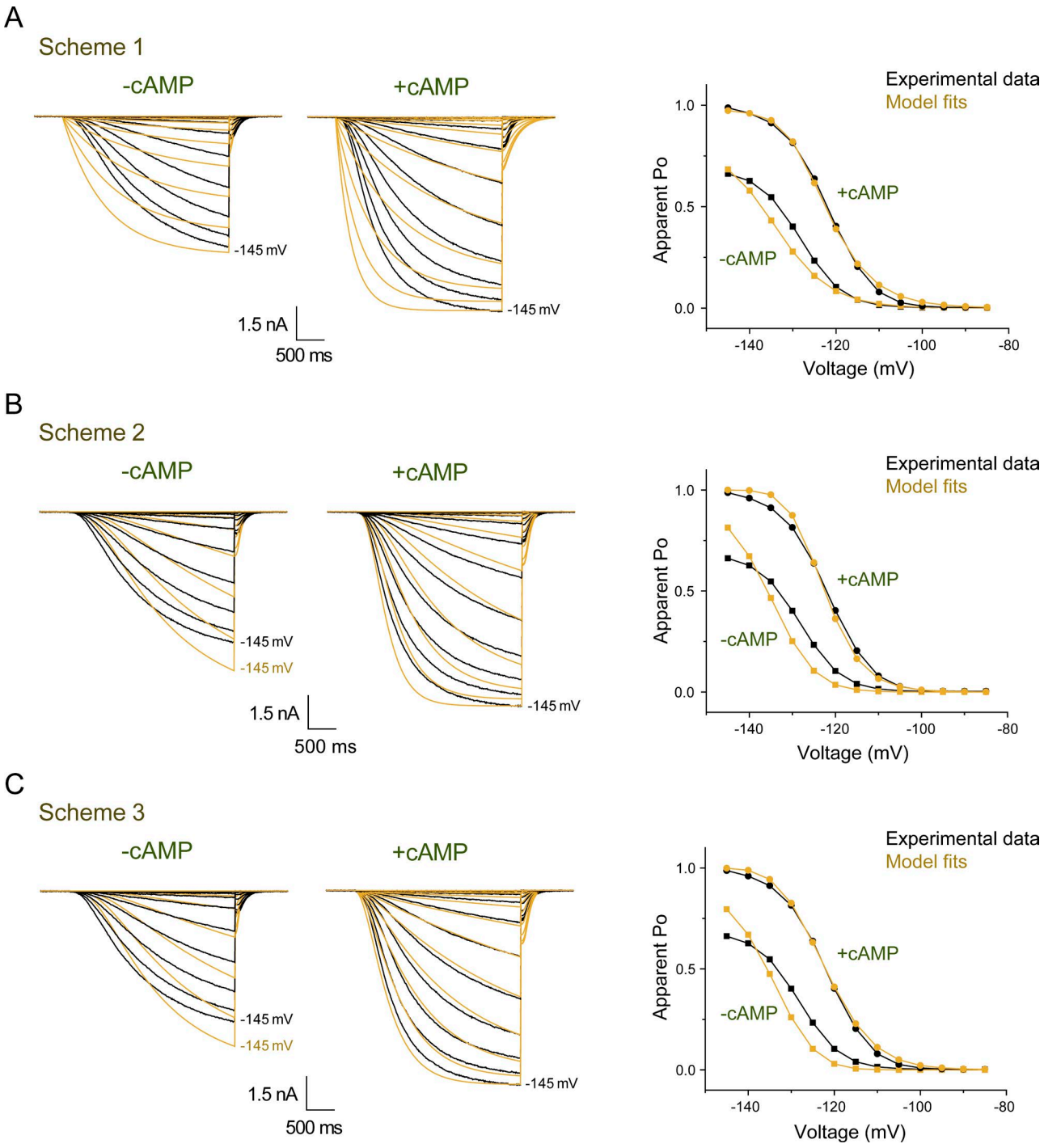

Figure S5. **Models lacking a linker domain did not describe the behavior of the HCN2/1 chimera. (A–C)** Model fits (yellow) and experimental data (black) for current traces in the presence and absence of cAMP for schemes lacking a linker domain. Only the interaction energies between the CNDB and the pore (Scheme 1–3), and pore and voltage sensors (Scheme 3) were allowed to change, keeping the rest of the parameters the same as for WT HCN2. Reference data for conductance–voltage curves (right) were obtained from the steady-state conductances calculated at the end of each pulse and are compared with the probability of the open state calculated for the model. Note the poor fit of the conductance–voltage curves in the absence of cAMP.

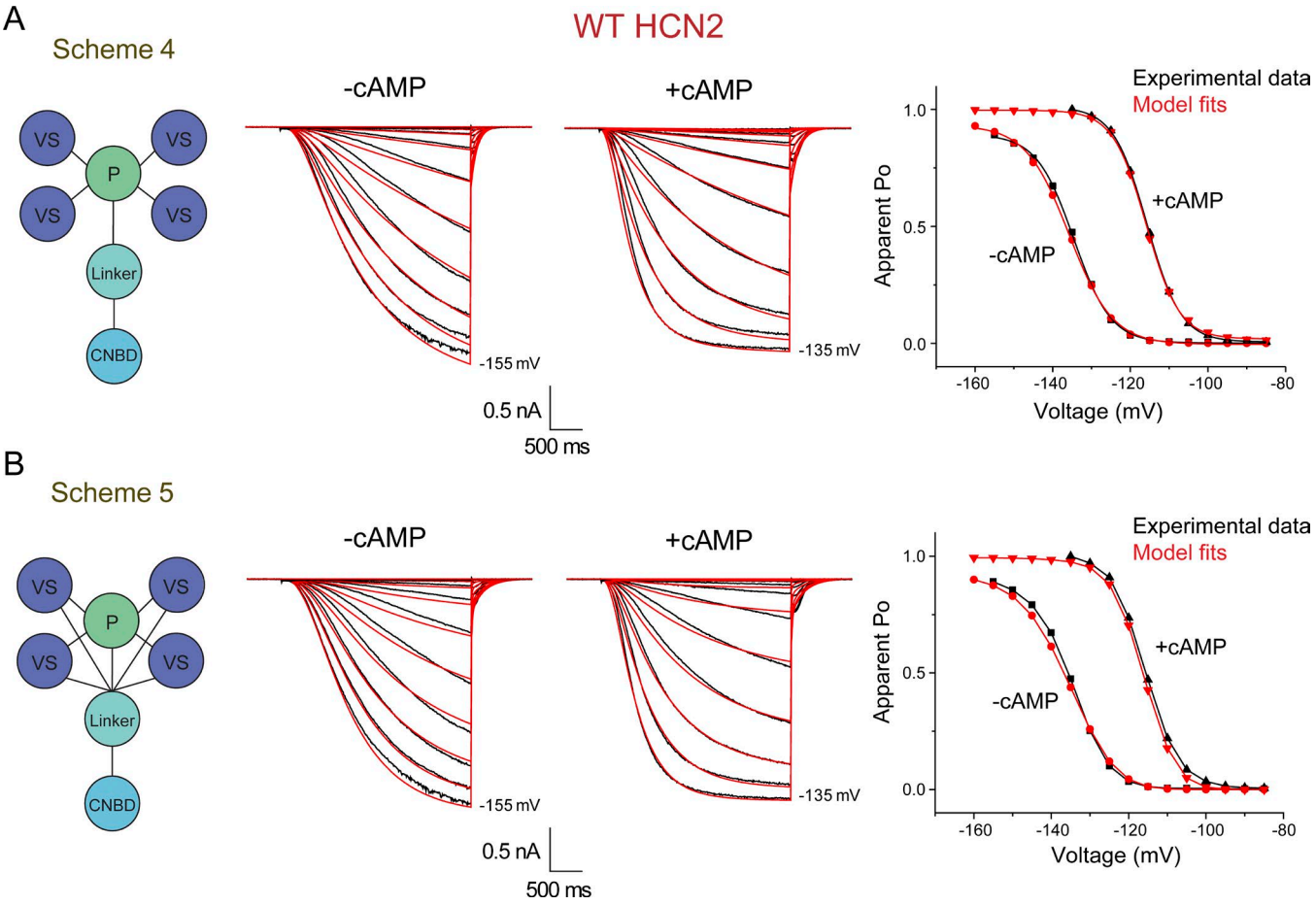

Figure S6. **Allosteric models of voltage- and ligand-dependent gating with a linker module.** Schematic representation of the elements and interactions implemented in Schemes 4 (A) and 5 (B) (left). Model fits (red) and reference traces (black) illustrating the activation kinetics in the presence and absence of cAMP. Reference data for the conductance-voltage curves (right) were obtained from the steady-state conductances calculated at the end of each pulse and are compared with the probability of the open state calculated for the model.

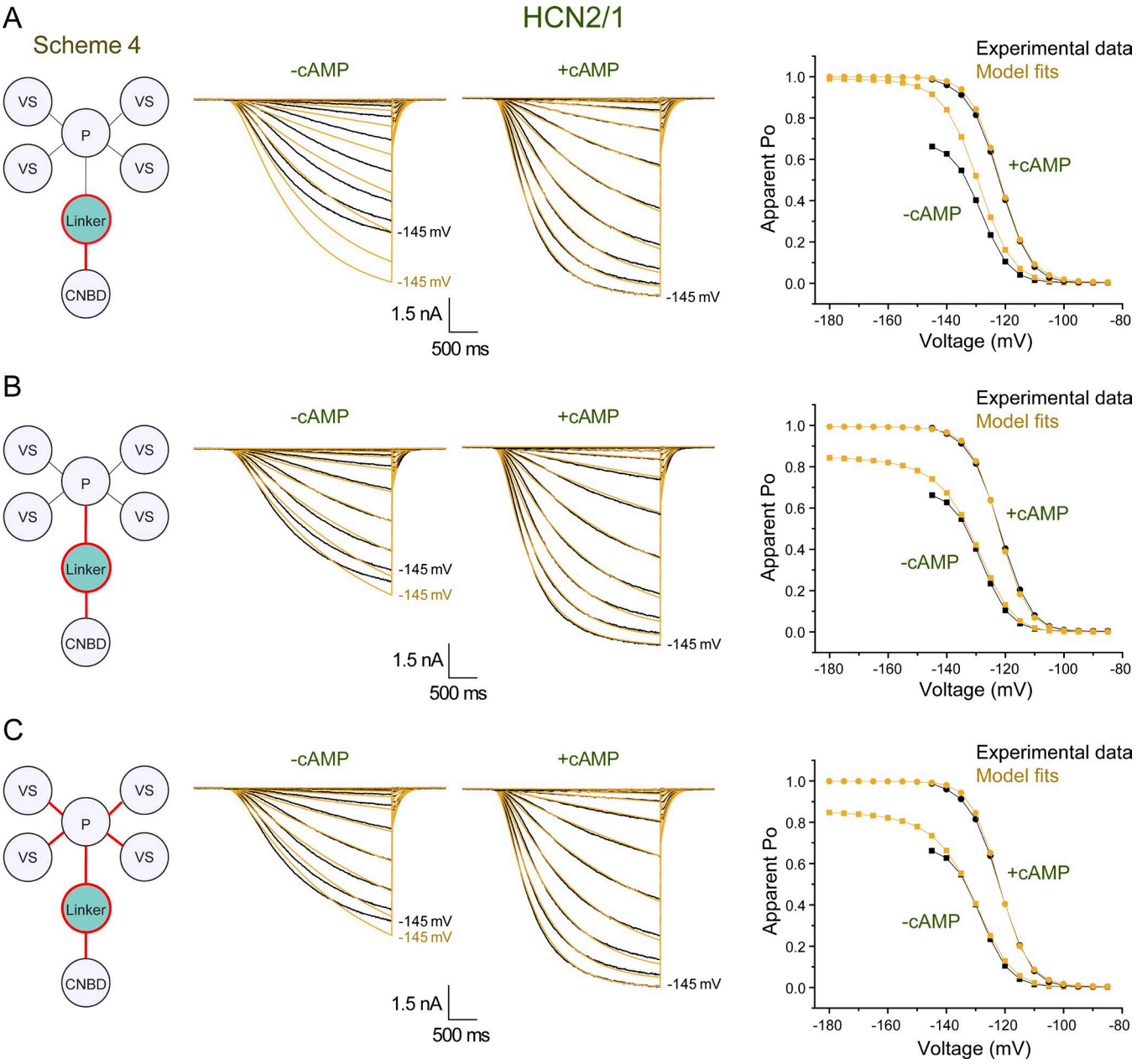

Figure S7. **Kinetic Scheme 4 described the behavior of the HCN2/1 chimera as well as that of WT HCN2.** To describe the HCN2/1 chimera, selected model parameters were altered as illustrated by red outlines on the left side diagrams; all other parameters remained the same as for WT HCN2. **(A)** The rate constants for the transitions of the linker and the interactions between the linker and the CNBD were optimized to fit current traces in response to voltage pulses and conductance–voltage curves in the presence and absence of cAMP for the HCN2/1 chimera. Model fits are shown in yellow and experimental data in black. Note the poor fit of the maximal current and conductance achieved by voltage alone (–cAMP). **(B)** Same as A, but additionally allowing changes in the interactions between the pore and the linker. Note the dramatic improvement of the fits, particularly in the absence of cAMP. **(C)** Same as B, but additionally allowing changes in the interactions between the pore and the voltage sensors. Note that the extra free parameters did not result in a noticeable improvement of the fits. Refer to Table S3 for a complete list of parameters.

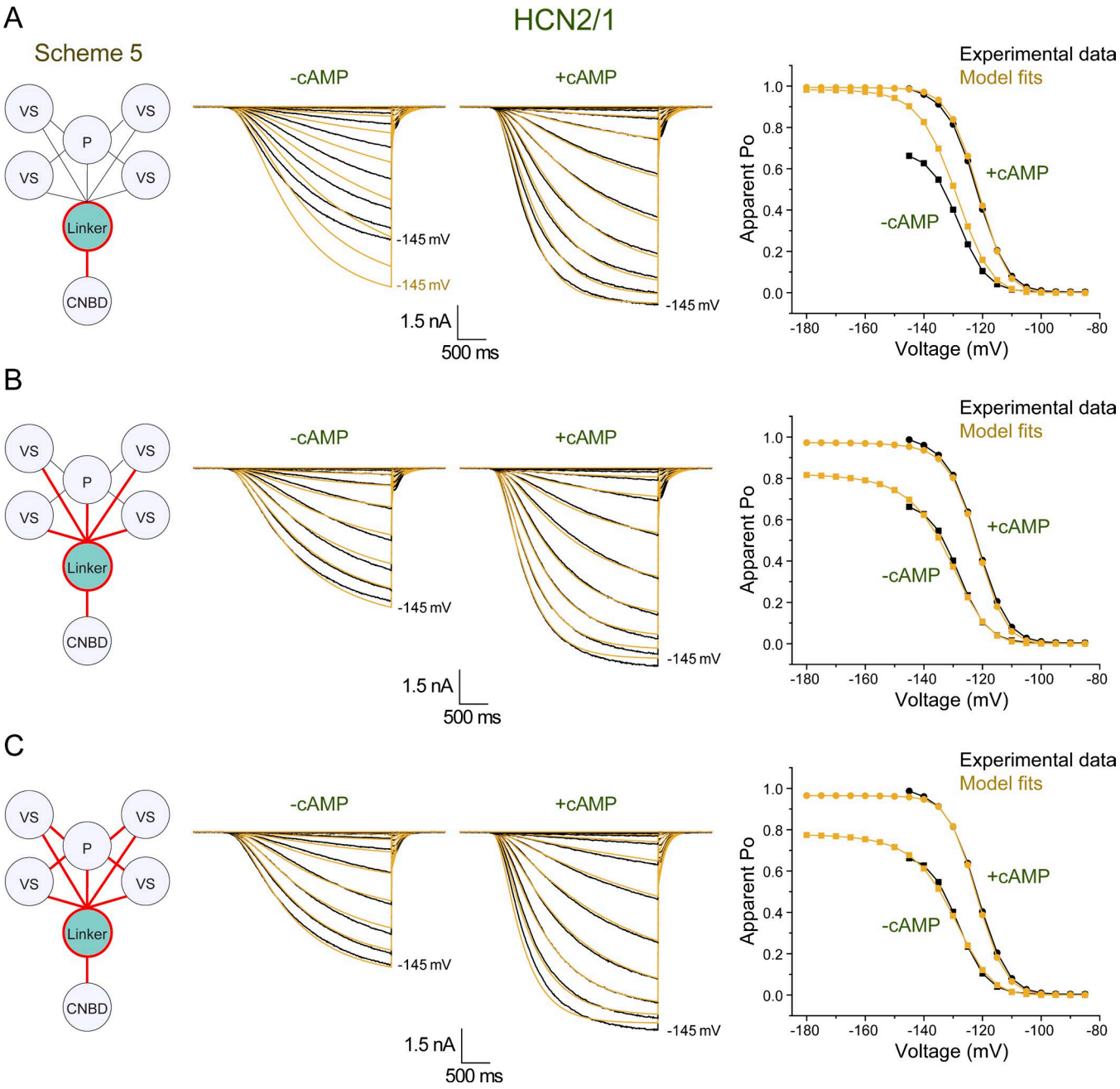

Figure S8. **Kinetic Scheme 5 is not a significant improvement over Scheme 4.** Scheme 5 is a Scheme 4 modified to introduce interactions of the linker with the four voltage sensors. Analogously to the fits to Scheme 4 in Fig. S7, the number of parameters that were allowed to deviate from the WT HCN2 values was progressively increased as indicated by red outlines in A–C. Model fits are shown in yellow and experimental data in black. **(A)** Note that the lack of optimization of the linker–pore interaction produces poor fit of the maximal current and conductance achieved by voltage alone (–cAMP). **(B)** In contrast to A, allowing the strength of the linker–pore and linker–voltage sensor interactions to vary produces very good fits. **(C)** Fits are not further improved when constraints on the pore–voltage sensor interactions are removed. Also note that despite the larger number of parameters, the fits afforded by Scheme 5 are not significantly better than those resulting from Scheme 4 (e.g., compare B with Fig. S7 B). Table S3 lists the values of all parameters used.

Table S1. **Voltage-dependent activation parameters with and without cAMP for HCN2 mutants carrying substitutions with HCN1 residues**

Number	Residues	−cAMP				+cAMP				$\Delta V_{1/2}$		*n*
		$V_{1/2}$		Slope		$V_{1/2}$		Slope				
		Mean	SEM	Mean	SEM	Mean	SEM	Mean	SEM	Mean	SEM	
	WT HCN2	−133.0	2.0	4.8	0.3	−114.2	2.0	4.6	0.1	18.8	0.6	19
1	D489E G493S G497D K534R	−128.5	2.0	5.5	0.3	−112.6	2.2	5.3	0.2	15.9	0.9	16
2	D489E G493S G497D	−129.8	1.6	5.4	0.2	−113.2	1.8	5.3	0.2	16.6	0.7	21
3	D489E G493S	−135.6	1.0	5.5	0.3	−117.5	0.9	5.3	0.3	18.1	0.8	21
4	K534R	−134.6	1.5	4.5	0.2	−117.3	1.3	4.8	0.2	17.3	0.5	18
5	D489E G493S G497D K534R S490N T549A I550V R588K	−127.4	1.7	5.8	0.4	−111.2	2.1	5.5	0.2	16.2	0.9	14
6	D489E G493S G497D K534R F469M M485I	−120.4	1.4	5.3	0.4	−109.2	1.7	4.9	0.2	11.2	0.7	13
7	F469M K534R	−135.7	1.2	5.1	0.2	−115.7	1.2	4.9	0.2	20.0	0.3	15
8	M485I K534R	−127.7	1.4	5.5	0.5	−114.0	1.3	4.9	0.3	13.7	0.7	14
9	D489E G493S G497D K534R S514T T531S	−124.5	1.3	5.0	0.3	−110.9	1.2	5.1	0.2	13.6	0.8	14
10	S514T K534R	−131.7	1.3	4.8	0.1	−116.3	1.1	4.6	0.1	15.4	0.4	19
11	T531S K534R	−134.1	0.9	5.9	0.4	−116.0	0.7	5.2	0.3	18.1	0.6	20
12	M485I G497D S514T	−124.2	0.9	5.4	0.2	−113.0	0.9	5.0	0.1	11.1	0.5	18
13	D489E G493S G497D K534R V562A S563G L565I G568S S575T	−123.3	1.1	4.5	0.2	−113.3	1.3	4.7	0.2	10.0	0.5	13
14	M485I G497D S514T V562A S563G	−123.1	1.2	5.1	0.2	−115.3	1.2	5.0	0.2	7.8	0.5	21
15	M485I G497D S514T L565I	−122.9	0.9	4.8	0.2	−113.1	0.7	4.7	0.1	9.9	0.4	22
16	M485I G497D S514T G568S	−124.7	1.0	4.9	0.3	−112.4	0.7	4.6	0.2	12.3	0.5	21
17	M485I G497D S514T S575T	−120.6	1.0	5.1	0.2	−111.3	0.7	4.8	0.1	9.2	0.6	21
18	M485I G497D S514T V562A S563G L565I	−118.9	1.3	5.7	0.3	−111.6	1.1	5.5	0.2	7.3	0.6	19
19	M485I G497D S514T V562A S563G S575T	−118.5	1.2	5.8	0.3	−111.1	0.9	5.6	0.2	7.4	0.6	18
20	M485I G497D S514T L565I S575T	−123.6	1.2	6.0	0.6	−114.1	1.0	5.7	0.4	9.6	0.6	17
21	M485I G497D S514T V562A S563G L565I S575T	−122.1	1.1	5.3	0.3	−114.8	0.9	5.1	0.2	7.3	0.7	20
	HCN2/1	−118.2	1.8	5.0	0.2	−111.1	1.6	5.1	0.4	7.2	0.6	19
	WT HCN1	−103.0	1.0	5.5	0.2	−99.6	1.0	4.7	0.3	3.4	0.4	21

Activation curves were generated from tail currents measured at −40 mV in inside-out macropatches. Currents in the absence and presence of 10 µM cAMP were measured in the same patch. *n* is the number of patches recorded per mutant.

Table S2. **Allosteric model parameters for WT HCN2**

		Scheme				
		1	**2**	**3**	**4**	**5**
Intrinsic rate constants						
Pore	C→O	2.50E-04	2.81E-04	2.77E-04	2.78E-03	5.03E-08
	O→C	2.00E+01	1.49E+04	1.90E+04	1.00E+01	3.04E+00
Each VS	R→A	3.60E-03	5.24E-04	7.03E-04	9.53E-02	2.68E-02
	A→R	5.04E+06	8.52E+03	5.95E+03	8.22E+04	3.85E+03
	R→A q	−3.21	−1.53	−1.48	−0.66	−−0.85
	A→R q	0.56	1.80	1.76	2.06	1.59
CNBD	U→B	1 [cAMP]	1 [cAMP]	1 [cAMP]	1 [cAMP]	1 [cAMP]
	B→U	0.001	0.001	0.001	0.001	0.001
Linker	R→A				1.32E-01	1.79E-01
	A→R				7.63E+01	2.13E+01
Interactions						
Pore–VS	$\Delta G^{\ddagger}_{pore-VS}$	−5.23	−1.23	−1.24	−1.58	−4.00
	$\Delta G_{pore-VS}$	−7.54	−4.52	−3.09	−4.00	−3.43
	$\Delta G^{\ddagger}_{VS-pore}$	−0.71	−2.18	−0.82	−5.12	−2.23
Pore–CNBD	$\Delta G^{\ddagger}_{pore-CNBD}$	−1.63	−3.05	−3.35		
	$\Delta G_{pore-CNBD}$	−1.72	−1.89	−4.75		
	$\Delta G^{\ddagger}_{CNBD-pore}$	0	0	0		
Pore–linker	$\Delta G^{\ddagger}_{pore-linker}$				2.77	6.91
	$\Delta G_{pore-linker}$				3.00	8.19
	$\Delta G^{\ddagger}_{linker-Pore}$				0	0
VS–CNBD	$\Delta G^{\ddagger}_{VS-CNBD}$			0.01		
	$\Delta G_{CNBD-VS}$			0.10		
	$\Delta G^{\ddagger}_{CNBD-VS}$			0		
VS–linker	$\Delta G^{\ddagger}_{VS-linker}$					0.24
	$\Delta G_{linker-VS}$					0.33
	$\Delta G^{\ddagger}_{linker-VS}$					0
Linker–CNBD	$\Delta G^{\ddagger}_{linker-CNBD}$				5.00	2.32
	$\Delta G_{linker-CNBD}$				7.00	8.64
	$\Delta G^{\ddagger}_{CNBD-linker}$				0	0
Derived equilibrium variables						
Pore	$K_{eq\ P}$	1.25E-05	1.89E-08	1.46E-08	2.78E-04	1.66E-08
VS	$K_{eq\ VS}$	7.14E-10	6.15E-08	1.18E-07	1.16E-06	6.96E-06
CNBD	$K_{eq\ CNBD}$	1,000 [cAMP]	1,000 [cAMP]	1,000 [cAMP]	1,000 [cAMP]	1,000 [cAMP]
Linker	$K_{eq\ L}$				1.73E-03	8.41E-03
Pore–VS	$\Theta_{pore-VS}$	336,057.76	2,069.66	185.35	862.17	329.68
Pore–CNBD	$\Theta_{pore-CNBD}$	18.35	24.25	3048.02		
Pore–linker	$\Theta_{pore-linker}$				6.31E-03	9.89E-07
VS–CNBD	$\Theta_{VS-CNBD}$			0.84		
VS–linker	$\Theta_{VS-linker}$					0.57
Linker–CNBD	$\Theta_{linker-CNBD}$				7.35E-06	4.60E-07

Rate constants - /s, charge (q) - e, ΔG - kcal/mol, [cAMP] - μm. Parameters for Scheme 1 were calculated from the eight-state allosteric model described in Chen et al. (2007); see Materials and methods). A, activated; B, bound, C, closed; $K_{eq} = k_{forward}/k_{reverse}$, interaction factor $\Theta = e^{-\Delta G/k_B T}$; O, open; R, resting; U, unbound; VS, voltage sensor.

Table S3. **Allosteric model parameters for the HCN2/1 chimera**

		Scheme								
		1	2	3	4			5		
					A	B	C	A	B	C
Intrinsic rate constants										
Pore	C→O	2.50E-04	2.81E-04	2.77E-04	2.78E-03	2.78E-03	2.78E-03	5.03E-08	5.03E-08	5.03E-08
	O→C	2.00E+01	1.49E+04	1.90E+04	1.00E+01	1.00E+01	1.00E+01	3.04E+00	3.04E+00	3.04E+00
Each VS	R→A	3.60E-03	5.24E-04	7.03E-04	9.53E-02	9.53E-02	9.53E-02	2.68E-02	2.68E-02	2.68E-02
	A→R	5.04E+06	8.52E+03	5.95E+03	8.22E+04	8.22E+04	8.22E+04	3.85E+03	3.85E+03	3.85E+03
	R→A q	−3.21	−1.53	−1.48	−0.66	--0.66	−0.66	−0.85	−0.85	−0.85
	A→R q	0.56	1.80	1.76	2.06	2.06	2.06	1.59	1.59	1.59
CNBD	U→B	1 [cAMP]	1 [cAMP]	1 [cAMP]	1 [cAMP]	1 [cAMP]	1 [cAMP]	1 [cAMP]	1 [cAMP]	1 [cAMP]
	B→U	0.001	0.001	0.001	0.001	0.001	0.001	0.001	0.001	0.001
Linker	R→A				5.45E-01	6.85E-01	6.63E-01	1.95E-01	7.04E-01	8.32E+00
	A→R				5.20E+00	7.45E+00	4.92E+00	3.08E+00	1.35E+01	3.90E+01
Interactions										
Pore–VS	$\Delta G^{\ddagger}_{pore-VS}$	−5.23	−1.23	−1.24	−1.58	−1.58	−1.48	−4.00	−4.00	−3.67
	$\Delta G_{pore-VS}$	−7.54	−4.52	−3.09	−4.00	−4.00	−2.40	−3.43	−3.43	−3.38
	$\Delta G^{\ddagger}_{VS-pore}$	−0.71	−2.18	−0.82	−5.12	−5.12	−1.20	−2.23	−2.23	0
Pore–CNBD	$\Delta G^{\ddagger}_{pore-CNBD}$	−0.79	−1.76	−3.63						
	$\Delta G_{pore-CNBD}$	−1.63	−2.41	−6.82						
	$\Delta G^{\ddagger}_{CNBD-Pore}$	0	0	0						
Pore–linker	$\Delta G^{\ddagger}_{Pore-Linker}$				2.77	7.42	5.02	6.91	6.55	7.57
	$\Delta G_{pore-linker}$				3.00	7.80	2.53	8.19	6.44	5.70
	$\Delta G^{\ddagger}_{linker-pore}$				0	0	0	0	0	0
VS–CNBD	$\Delta G^{\ddagger}_{VS-CNBD}$			0						
	$\Delta G_{CNBD-VS}$			0.88						
	$\Delta G^{\ddagger}_{CNBD-VS}$			0.66						
VS–linker	$\Delta G^{\ddagger}_{VS-linker}$							0.24	−0.14	−0.20
	$\Delta G_{linker-VS}$							0.33	−0.08	−0.30
	$\Delta G^{\ddagger}_{linker-VS}$							0	−0.04	0
Linker–CNBD	$\Delta G^{\ddagger}_{Linker-CNBD}$				0.37	0.26	0.42	0.53	0.34	6.92
	$\Delta G_{linker-CNBD}$				0.98	1.01	1.10	1.07	1.20	2.99
	$\Delta G^{\ddagger}_{CNBD-linker}$				0	0	0	0	0	0
Derived equilibrium variables										
Pore	$K_{eq\ P}$	1.25E-05	1.89E-08	1.46E-08	2.78E-04	2.78E-04	2.78E-04	1.66E-08	1.66E-08	1.66E-08
VS	$K_{eq\ VS}$	7.14E-10	6.15E-08	1.18E-07	1.16E-06	1.16E-06	1.16E-06	6.96E-06	6.96E-06	6.96E-06
CNBD	$K_{eq\ CNBD}$	1,000 [cAMP]	1,000 [cAMP]	1,000 [cAMP]	1,000 [cAMP]	1,000 [cAMP]	1,000 [cAMP]	1,000 [cAMP]	1,000 [cAMP]	1,000 [cAMP]
Linker	$K_{eq\ L}$				1.05E-01	9.19E-02	1.35E-01	6.32E-02	5.21E-02	2.13E-01
Pore–VS	$\Theta_{pore-VS}$	336,057.76	2,069.66	185.35	862.17	862.17	57.08	329.68	329.68	303.19
Pore–CNBD	$\Theta_{pore-CNBD}$	15.70	58.46	99,590.04						
Pore–linker	$\Theta_{pore-linker}$				6.31E-03	1.89E-06	0.01	9.89E-07	1.90E-05	6.55E-05
VS–CNBD	$\Theta_{VS-CNBD}$			0.22						
VS–linker	$\Theta_{VS-linker}$							0.57	1.14	1.66
Linker–CNBD	$\Theta_{linker-CNBD}$				0.19	0.18	0.15	0.16	0.13	0.01

Rate constants - /s, charge (q) - e, ΔG - kcal/mol, [cAMP] - μm. A, activated; B, bound, C, closed; $K_{eq} = k_{forward}/k_{reverse}$, interaction factor $\Theta = e^{-\Delta G/k_B T}$; O, open; R, resting; U, unbound; VS, voltage sensor.

Table S4. **Allosteric model parameters for the $HCN1_{minimal}$ mutant: Schemes 4 and 5**

		Scheme		
		4	5	
		B	B	C
Intrinsic rate constants				
Pore	C→O	2.78E-03	5.03E-08	5.03E-08
	O→C	1.00E+01	3.04E+00	3.04E+00
Each VS	R→A	9.53E-02	2.68E-02	2.68E-02
	A→R	8.22E+04	3.85E+03	3.85E+03
	R→A q	-0.66	-0.85	-0.85
	A→R q	2.06	1.59	1.59
CNBD	U→B	1 [cAMP]	1 [cAMP]	1 [cAMP]
	B→U	0.001	0.001	0.001
Linker	R→A	4.82E-01	2.65E-01	2.65E-01
	A→R	1.66E+00	1.35E+00	1.35E+00
Interactions				
Pore–VS	$\Delta G^{\ddagger}_{pore-VS}$	-1.58	-4.00	-3.97
	$\Delta G_{pore-VS}$	-4.00	-3.43	-3.61
	$\Delta G^{\ddagger}_{VS-pore}$	-5.12	-2.23	-1.98
Pore–linker	$\Delta G^{\ddagger}_{pore-linker}$	5.50	6.03	5.33
	$\Delta G_{pore-linker}$	6.00	2.73	5.82
	$\Delta G^{\ddagger}_{linker-pore}$	0	0	0
VS–linker	$\Delta G^{\ddagger}_{VS-CNBD/linker}$		-0.30	-0.12
	$\Delta G_{CNBD/linker-VS}$		-0.46	-0.53
	$\Delta G^{\ddagger}_{CNBD/linker-VS}$		0	0
Linker–CNBD	$\Delta G^{\ddagger}_{linker-CNBD}$	0	-2.85	4.95
	$\Delta G_{linker-CNBD}$	3.33	9.29	3.09
	$\Delta G^{\ddagger}_{CNBD-linker}$	0	0	0
Derived equilibrium variables				
Pore	$K_{eq\ P}$	2.78E-04	1.66E-08	1.66E-08
VS	$K_{eq\ VS}$	1.16E-06	6.96E-06	6.96E-06
CNBD	$K_{eq\ CNBD}$	1,000 [cAMP]	1,000 [cAMP]	1,000 [cAMP]
Linker	$K_{eq\ L}$	2.91E-01	1.97E-01	1.97E-01
Pore–VS	$\Theta_{pore-VS}$	862.17	329.68	445.07
Pore–linker	$\Theta_{pore-linker}$	3.98E-05	9.95E-03	5.43E-05
VS–linker	$\Theta_{VS-linker}$		2.16	2.44
Linker–CNBD	$\Theta_{linker-CNBD}$	3.63E-03	1.54E-07	5.41E-03

Rate constants - /s, charge (q) - e, ΔG - kcal/mol, [cAMP] - µm. A, activated; B, bound, C, closed; $K_{eq} = k_{forward}/k_{reverse}$, interaction factor $\Theta = e^{-\Delta G/k_B T}$; O, open; R, resting; U, unbound; VS, voltage sensor.

References

Chen, S., J. Wang, L. Zhou, M.S. George, and S.A. Siegelbaum. 2007. Voltage sensor movement and cAMP binding allosterically regulate an inherently voltage-independent closed-open transition in HCN channels. *J. Gen. Physiol.* 129:175–188. https://doi.org/10.1085/jgp.200609585